- Technical Paper -

ANALYTICAL INVESTIGATION ON STRESS TRANSFER IN EPOXY ADHESIVE ANCHOR UNDER TENSION

Hui GAO[*1] and Ayumi SATOH[*2]

ABSTRACT

The authors investigated experimentally and analytically a M12 bolt anchor fixed with epoxy adhesive measuring the length L=100 mm and the drilled hole diameter D=14 mm. A pullout-resistant model was presented and the ratios of supported load were calculated among three constituents in the model at the peak load. Moreover, the stress transfer mechanisms from the bolt surface to the concrete was discussed including the features of the stress transfer through the adhesive-concrete interface. The influence of the bearing plate and the contribution of σ_{zz} to the failure were also discussed.

Keywords: post-installed anchor, epoxy, FEM analysis, failure mechanisms, combined failure.

1. INTRODUCTION

Epoxy adhesive anchor is an indispensable material used worldwide for equipment fixing, reinforcing and retrofitting of RC member of the structure. Recently the design guidelines were updated [1] and the regulation regarding the strength of the anchor was newly designated [2]. Thus the adhesive anchor is expected to be increasingly used for many purposes.

The authors have been investigating [3][4] with the intention of enhancing the mechanical performance of the adhesive anchor with a relatively short embedment length. One of the most innovative ideas for that purpose would derive from the basic study of the stress transfer and failure mechanisms.

The characteristic of the authors' research at investigating these issues is based on a new viewpoint: 'Mesoscopic materials engineering' where FEM analysis is regarded as a numerical experiment to obtain otherwise unknowable information and consider the results as important as the results from a real experiment.

There are numerous studies, including FEM analysis for the adhesive anchor. Li et al. conducted a study [5] that formulated FEM models for predicting the pullout capacity of anchors (expansive type of mechanical anchor and adhesive anchor) of a specific manufacturing company. There was a study by Barnat [6] in which non-linear FEM analysis of 3D models was employed. It predicted how the pullout capacity of the epoxy adhesive anchor (the used bolt was M12 in diameter and 110 mm long: L/d is 9.2) would change according to the strength of substrate concrete, and these analytical results were experimentally confirmed. As for the analytical study regarding the bond behavior, Upadhyaya and Kumar [7] conducted the analysis with using two fourth order partial differential equations and FEM analysis. They revealed the mechanics of stress transfer through the adhesive layer. Wang et al. [8] studied post-installed large-diameter anchors to formulate the pullout capacity of them. Also, they discussed the failure mode, the suitable groove of the bars and the effects of the large diameter.

Regarding the failure mechanisms without employing FEM analysis, there is a Cook's equation [9]. He predicted the depth of the main crack initiation by employing the shear stress along the adhesive layer and the tensile stress through the surface of imaginary cone surface of concrete that would fracture.

Other than those researches, many researches so far are based on experiments. Among them, Kasa et al. [10] discussed the load-bearing mechanisms based on the experiment and clarified the embedded length that changes the cone failure into the combined failure was 3d~6d (d: bolt diameter).

Among the above mentioned previous studies that involve FEM analysis, there is no study that use the FEM results for expressing the stress transfer from bolt to bearing plate. This paper focuses on the issue with employing one case of epoxy adhesive anchor (L=100 mm, d=12 mm, D=14 mm) under tension. Abbreviated words used are listed in Table 1.

Table 1 Nomenclature.

Abb.	Description
A0	Point in the middle of adhesive layer
AC i/f	Interface between adhesive and concrete
ACC	Concrete element adjacent to AC interface
BA i/f	Interface between bolt and adhesive
BAB	Bolt element adjacent to BA interface
d	Nominal diameter of a bolt
D	Diameter of drilled hole
Fc	Compressive strength of concrete
Ft	Tensile strength of concrete
L	Effective embedded length
S_a	Maximum principal axial stress in xy-plane
S_b	Minimum principal axial stress in xy-plane

*1 Graduate School of Engineering, Kumamoto University, JCI Student Member
*2 Associate Prof., Faculty of Advanced Science and Technology, Kumamoto University, Dr.E., JCI Member

2. EXPERIMENT AND ANALYSIS

As for the detail of experiment and FEM analysis, please refer to the references [3] [4]. In this paper, only the essential outline is written.

The shape and dimensions of the adhesive anchor and the pullout test setup are shown in Fig.1. The substrate is a concrete block measured ϕ=300 mm and h=150 mm. The concrete was 'Ordinary-24-18-20-N' with the measured strengths Fc=33.6 MPa and Ft=3.12 MPa. The bolt was SNB7 all-thread M12 bolt with the measured strength Ft=1083 MPa. The adhesive was high viscosity epoxy resin with the measured strengths Fc=69.9 MPa and Ft=39.1 MPa.

After the M12 bolt was fixed in the drilled hole (D=14 mm, L=100 mm) with epoxy, the anchor was pulled out with a center-hole jack.

FEM analysis was performed using the general-purpose nonlinear structural analysis software DIANA 10.6. The element partitioning diagram of the analyzed model is represented in Fig. 2. Constitutive laws generally follow the reference [3], but the spring coefficients for the AC i/f were newly determined after many trial and error procedures. The used i/f properties are shown in Table 2. Compressive behavior of concrete follows the Popovics equation with Fc=33.6 MPa and tensile behavior follows JSCE's 1/4 model with Ft=3.12 MPa and fracture energy=0.1 N/mm.

3 RESULTS

The failure mode was a combined failure. The detail of the specimen after failure is shown in Fig. 3. The depth of the concrete cone was 70 mm in the left half and 30 mm in the right half (Fig. 3a,b). There were several radial cracks on the surface that are indicated by yellow arrows in Fig. 3c. These radial cracks did not penetrate the substrate.

Fig. 4 shows the load-displacement curve. After the peak load, the load suddenly decreased and the measurement was out of record till 7.5 mm (as dotted line indicates) due to the cone failure of concrete.

Fig. 5 represents crack patterns and principal stress contours. Because S1 in Fig. 5 includes σ_{zz} (if it is the max. stress), max. principal stress in xy-plane (S_a) should have another appearance. For example, the large high tensile stress region above 2.08 MPa at the peak load is owing to σ_{zz} which is shown in Fig. 10(a) From Fig.6(b), the region near the main crack would be about 1.49 MPa on average. S3 in Fig. 5 also includes σ_{zz} (if it is the min. stress). But compressive σ_{zz} which is later shown in Fig. 10(b) occupies a small region near the bolt. Therefore the region above the main crack is regarded as a compressive strut to support the pullout load.

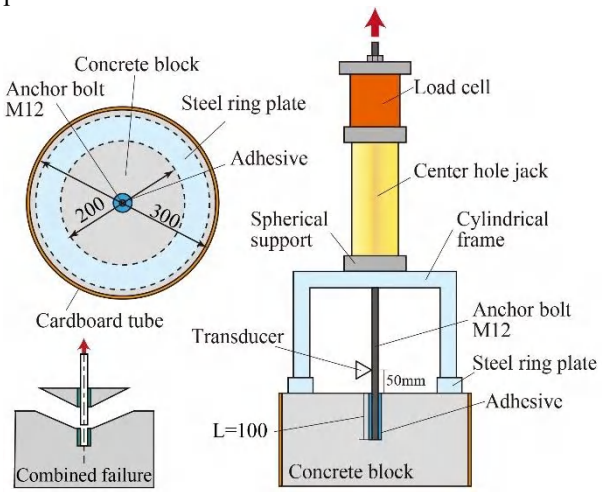

Fig.1 Test setup and failure mode of anchor.

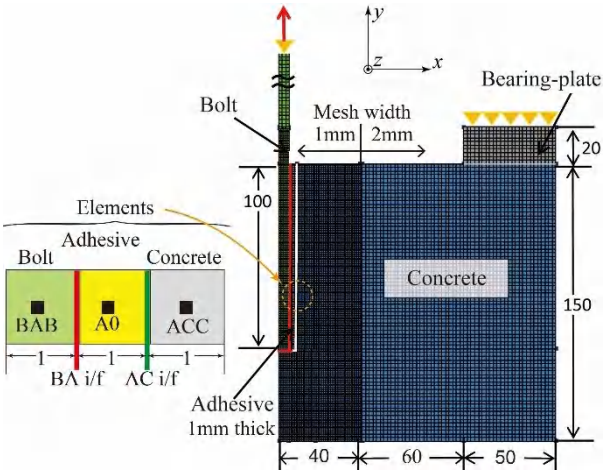

Fig.2 FEM mesh and coordinate system.

Table 2 Properties of BA and AC interface.

Bond strength (MPa)		Spring coefficient (MPa/mm)	
BA i/f	AC i/f	BA i/f	AC i/f
>24.0	24.0	50.0	40.0

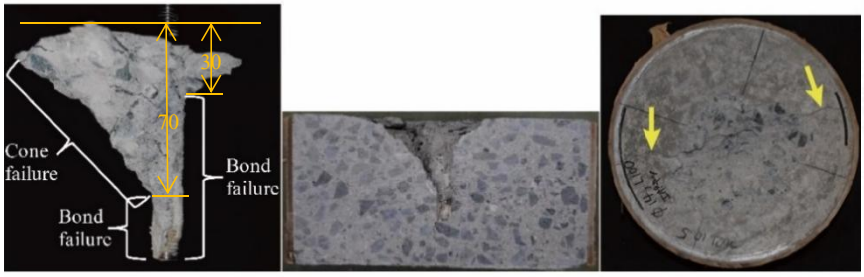

(a) Pulled-out anchor (b) Cut substrate after pullout (c) Surface after pullout

Fig.3 Observation of the tested anchor.

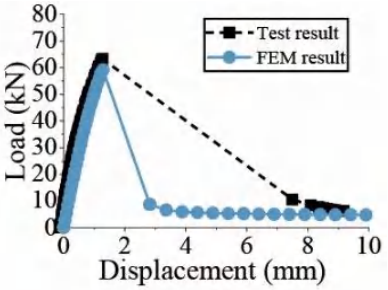

Fig.4 Load-displacement curve.

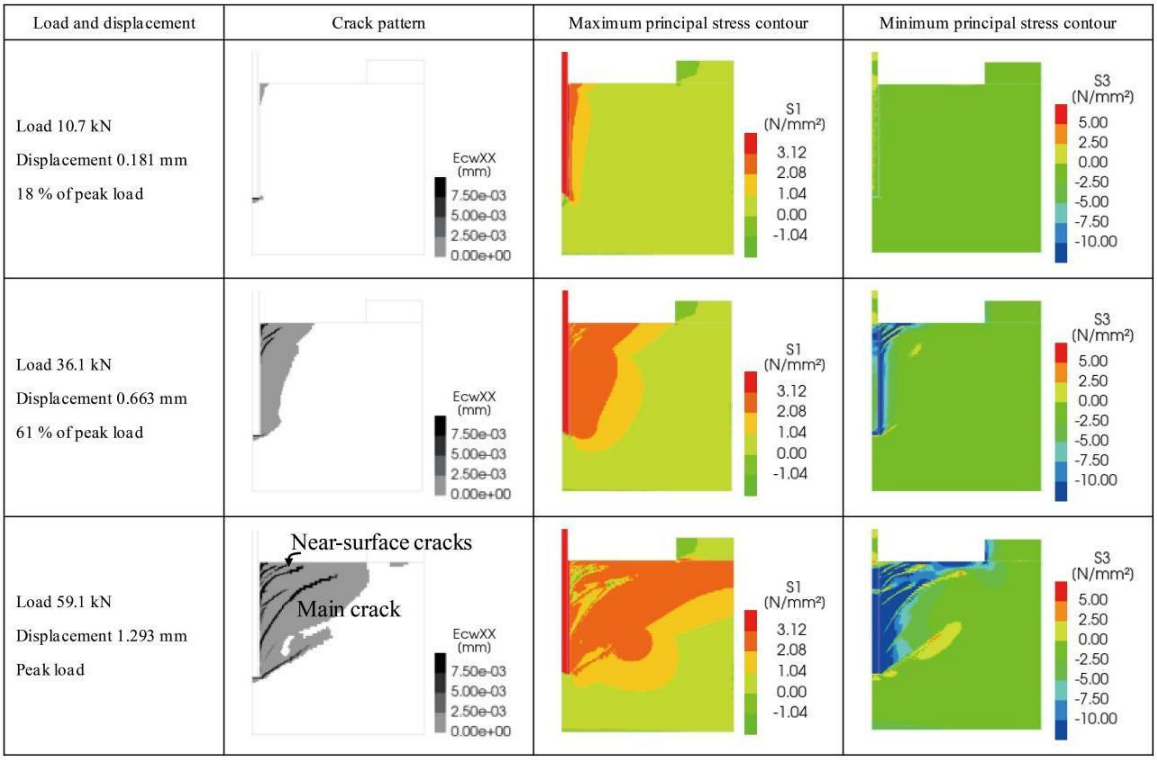

Fig.5 Crack pattern and maximum and minimum principal stress.

4. DISCUSSION

4.1 Load-bearing macro-model

(1) Macro model

Fig.6 shows a load-bearing model which is the redrafted one from the reference [4]. A part of concrete above the surface crack is excluded from bearing the load, written 'void' in the figure. A part of concrete under the main crack is regarded as the stable 'substrate'. A part between them supports the load by forming a 'conical arch'. The upper part of the conical arch extending to the bearing-plate is regarded as a thick disc-like beam, which is written 'circular beam'. A cylindrical section vertically above the crack tip is indicated with dotted line and called 'ligament'. There is also a dotted line located between ligament and the end of the bearing plate. This cylindrical section is used for an imaginary failure section of the circular beam.

(2) Calculation of F1, F2 and F3

F1, F2 and F3 were calculated in the same way as the reference [3].

$$F1 + F2 + F3 = P \quad (1)$$

$$F1 = \sum 2\pi r h \tau_{xy} \quad (2)$$

$$F2 = \sum T_a \cos\theta, \quad T_a = S_a A \quad (3)$$

$$F3 = \sum 2\pi R H \tau_{xy(Cb)} \quad (4)$$

where,

r: radius measured from the bolt center

h: divided length of the segment of AC i/f

τ_{xy} : shear stress

$\tau_{xy(Cb)}$: shear stress that exists at Circular beam

S_a: max. principal stress in the conical arch

A: area of the segment

θ: angle of the segment of the crack

R: radius measured from the bolt center

H: divided height of the ligament

The distribution of S_a and τ_{xy} in ACC is depicted in Fig.6(b) and 6(c) respectively.

When calculating F2, the representative point for every segment along the main crack was determined to be evenly located at about 10 mm.

(3) Load-bearing shares

The calculated forces and the share ratio of the component is summarized in Table 3.

In this table, another case of F3 was added (as 'F3 by strength'), which is calculated by multiplying the shear strength (2.58 MPa = 1/13 Fc) with the cylindrical surface area at the imaginary fracture section of the circular beam. The shear strength 2.58 MPa for the prediction was surmised with considering that the cylindrical section was under tension softening region and also subject to large σ_{zz}.

Because 'F3 by stress' was predicted based on the assumption that it was supported only by shear stress at the ligament of the circular beam and excluded the y-directional contribution of the axial stress, it is substantially small.

Table 3 Experimental and predicted max. loads.

Experi-	Predicted (kN)				Predicted /
ment	F3 by stress	F2	F1	Sum	Experiment
63.2	6.4 (12%)	27.3 (52%)	18.8 (36%)	52.5	0.83
	F3 by strength				
	12.9 (22%)	27.3 (46%)	18.8 (32%)	59.0	0.93

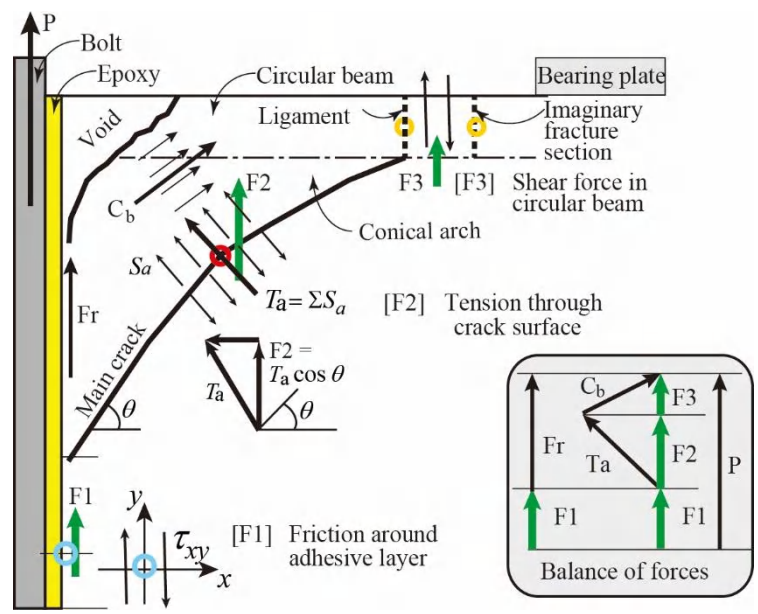

(a) Load bearing forces comprised of F1, F2 and F3[4].

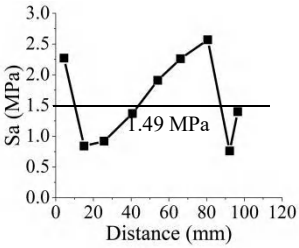

(b) S_a for calculation of F2.
(Distance 0 is the crack tip)

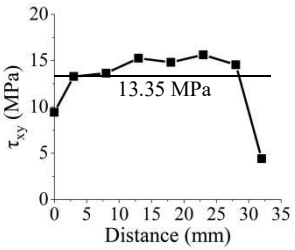

(c) τ_{xy} for calculation of F1
(Distance 0 is the start point of main crack)

Fig.6 Load bearing mechanisms: Forces, their balance and stress distribution of comprising forces.

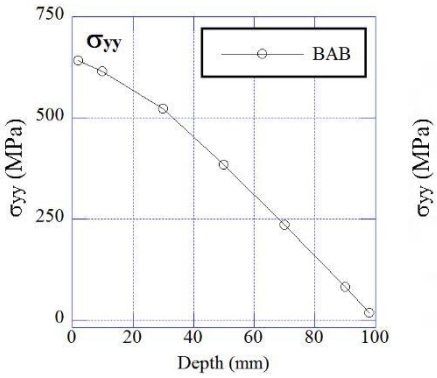

(a) σ_{yy} for BAB

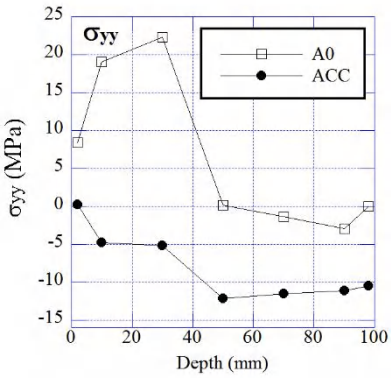

(b) σ_{yy} for A0 and ACC

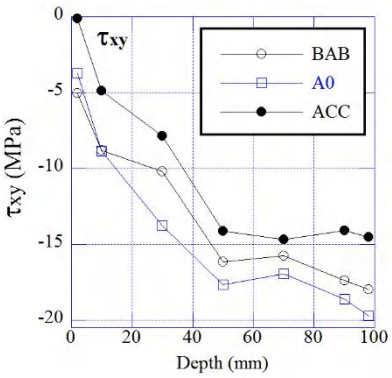

(c) τ_{xy}

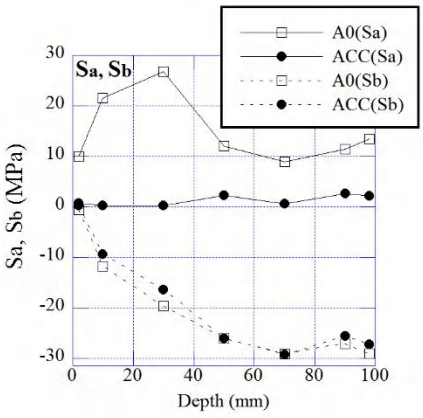

(d) S_a and S_b

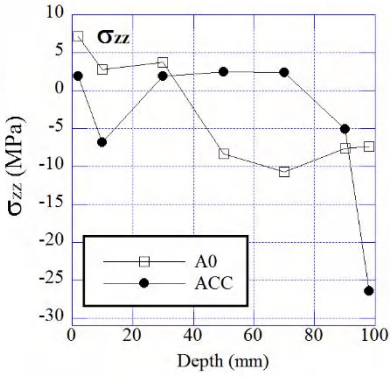

(e) σ_{zz}

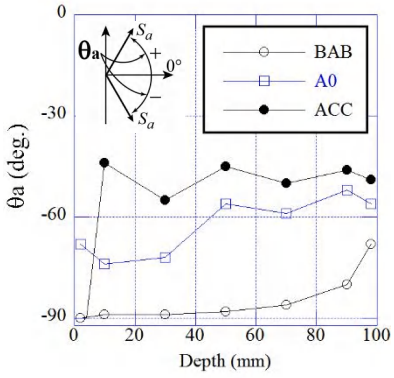

(f) θ_a

Fig.7 Stresses and θ_a along the depth from bolt surface to concrete surface adjacent to the interface.

4.2 Load transfer from bolt to concrete

Figs. 7 display characteristic values regarding stress transfer from bolt to concrete at the peak load. BAB, A0 and ACC mean the bolt element adjacent to BA i/f, the middle of the adhesive layer and the concrete element adjacent to AC i/f respectively.

The surface cracks make the τ_{xy} near the surface low (Fig. 7(c)) affecting the inclination of σ_{yy} at BAB (Fig. 7(a)). σ_{yy} near the surface at A0 is high (Fig. 7(b)) for offsetting the low τ_{xy}. But the max. principal stress (S_a) is well below the tensile strength of it ((Fig. 7(d)). It should be noted that min. principal stress (S_b) is near

the compressive strength at ACC, and is even below 50 mm from the surface ((Fig. 7(d)) making this part the conical arch referred to Fig. 6.

It is found that σ_{zz} at the middle depth of ACC is near the tensile strength of concrete ((Fig. 7(e)). At the same time σ_{zz} at the bottom indicates high compressive stress which corresponds to the high compressive stress spot shown in Fig. 10(b).

From θ_a ((Fig. 7(f)) which is the orientation angle of S_a, it is obvious that the angle changes from -90° at BAB to -45° at ACC and the angle at A0 is about -60°. This means the adhesive layer functions as an orientation changer. Because the orientation angle of S_b is +45° (i.e, S_a+90°), S_b in Fig. 7(d) is effective as a compressive strut C_b as shown in Fig. 6.

Fig. 8 shows the stress circle at the depth where the main crack initiated (68 mm) when the peak load. Ntr and Str mean the normal stress to the i/f and the traction through the i/f respectively, and they are the output values from DIANA. The location of A0, AC i/f and ACC is depicted in the lower right of Fig. 8. Ntr is the x-axial stress and Str is the shear stress at the i/f.

Therefore, it is natural that the solid green point (that indicates the stress (Ntr, Str) at AC i/f) is located near the red solid points (that indicate the stress (σ_{xx}, τ_{xy}) at A0 and ACC).

4.3 Failure mode

(1) Penetrating surface crack

Figs.9(a, b) show the crack patterns of the tested anchor. At the peak load, one surface crack penetrated but the main crack only reached the point (78,10) in xy-coordinate. At the post-peak load, the concrete above the penetrating crack fractured and at the same time ACC (concrete adjacent to AC i/f) failed with accompanied by the bolt pullout.

It should be noted that the bond stress at AC i/f did not reached the bond strength at the peak load. (From Fig. 7(c) the bond stress is about 15 MPa.) This failure mode is traditionally called combined cone (penetrating surface crack) and bond (below the penetrating crack) failure, which corresponds to the photo of the left half in Fig. 3(a).

But the real trigger of the failure is cone fracture of the surface crack and the bond failure is the secondary one.

(2) Contribution of σ_{zz} to main crack failure

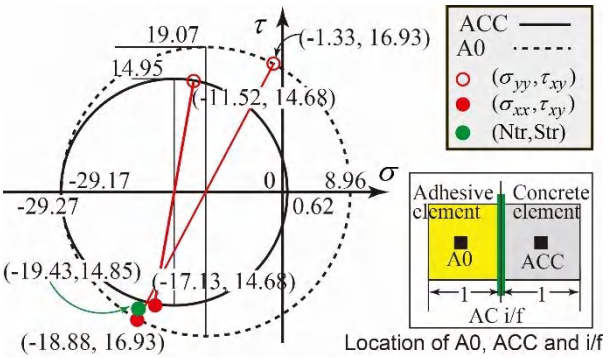

Fig.8 Stress change from A0 to ACC via AC i/f.

Fig.10 represents σ_{zz} contour at the peak load where a wide range of large tensile stress part (colored in orange) appears near the surface and a large compressive part at the bottom of the substrate making a pair for balancing forces. Also, a tensile part emerges below the main crack and a compressive part above the bottom crack making a pair (Fig.10(c)). These are based on the same mechanisms that govern the splitting of surrounding concrete by deformed bar in RC member. But in the anchor, as the tensile σ_{zz} exists only near the surface, radial cracks occur accordingly. The arrows in Fig.3(c) show this radial cracks.

The final failure occurred at the zone which was marked “failed” in Fig.10(a). This zone lies in high tensile σ_{zz} region as Fig.10(a) shows, and it also corresponds to the tension softening region as Fig.9(a) shows. So the “failed” zone was subjected to high tensile stress not only in xy-plane but also in z direction. Thus, the main crack easily penetrates through the region triggered by the expansion of surface crack or other small changes of stresses. This is the reason for the combined failure of the left half of Fig.3(a).

This type of failure is generally called the combined failure, but the bond failure is also the secondary one as discussed in the previous section. Therefore this type of combined failure would be called cone failure reflecting the real trigger of the failure.

A high compressive stress spot is found at the bottom of ACC (concrete adjacent to AC i/f). This spot may bring the similar confinement effect like hoop bars in reinforced concrete.

Hence the contribution of σ_{zz} to the failure is significant.

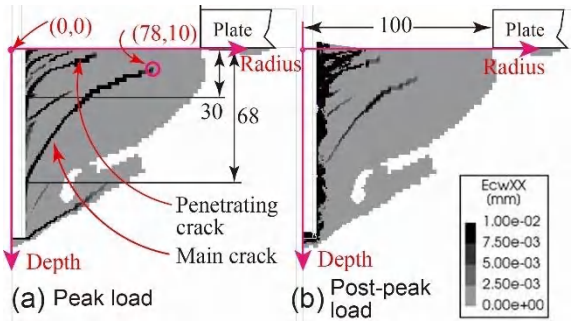

Fig.9 Crack patterns.

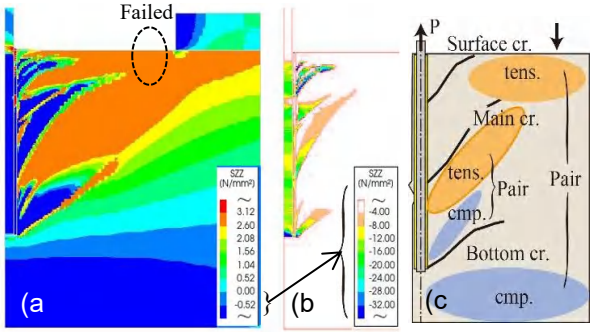

Fig.10 σ_{zz} contour: (a) for tensile., (b) for compressive part, (c) for schematic interpretation of (a) and (b).

4.4 Influence of bearing plate

Fig. 11(a) represents analyzed results of 'R300 model' which has a different boundary condition from the one depicted in Fig. 5. 'R300 model' was fixed at circumference surface, whereas the model depicted in Fig. 2 called 'B. Plata model' is vertically supported at the top of base plate. 'R300 model' is an imitating of the anchor fixed in very large solid substrate. 'R300 model' has a narrower region of tensile softening region than 'B. Plate model'.

Fig. 11(b) represents the crack pattern at the peak load. Though the surface cracks are almost the same pattern as the one shown in Fig. 9(a), the main crack in Fig. 11(b) is deeper than the one in Fig. 9(a).

Fig. 11(c) represents the load-displacement curves of 'R300 model' and 'B. Plate model'. The pullout capacity of the former was 54.14 kN, whereas the latter was 59.13 kN (showing 9 % of increase).

Fig. 11(d) represents the min. principal stress contour of this model. Though the depth of the main crack is different from that of Fig. 5, the conical arch in Fig 11(d) and Fig. 5 are extending to the similar distance (100 mm). It means that the conical arches which support the main part of the load are similar. Thus the difference of pullout capacity between these models fell within about 10%.

5. CONCLUSIONS

M12 bolt anchor with an embedment length of 100 mm fixed with epoxy adhesive was investigated.

The findings are:

(1) A load-bearing macro model, which consists of F1, F2 and F3, was confirmed.
F1: Load supported by bond stress around AC interface occupied 12% of the peak load.
F2: Load supported by tensile stress through a conical crack in concrete occupied 52%.
F3: Load supported by an imaginary disk-shaped beam (circular beam) near the surface of concrete occupied 36%, if F3 was calculated with the shear stress in the ligament of the circular beam.

(2) There is a wide region of high tensile σ_{zz} near the surface of the substrate. This would affect the shear strength of the circular beam.

(3) The failure mode of the anchor was a generally-called 'combined failure'. But the shear stress at the peak load was below the shear strength around the interface.

(4) The bearing plate that supported the load would have increased the pullout capacity up to 10%, which was confirmed by a model with another boundary conditions.

ACKNOWLEDGEMENT

This study was supported by the China Scholarship Council Program [Project ID:202308050051] and JSPS KAKENHI Grant Numbers 20K04772, 23K17790. The authors greatly appreciate the insightful discussions with Professor emeritus K. Yamada, whose contributions were deeply inspiring.

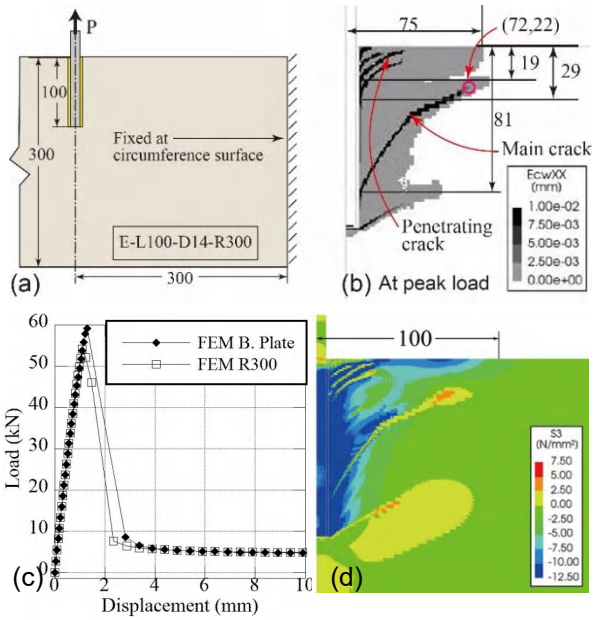

Fig. 11 Analyzed results of R300 model.

REFERENCES

[1] AIJ, Design Recommendations for Composite Constructions. AIJ, Tokyo, Japan, Revised 2023.

[2] KokuJyuuSi-1597, Ministry of Land, Infrastructure, Transport and Tourism, 2022.

[3] A. Satoh and K. Murakami, Analytical Study on Fracture Mechanisms Ruling Resistant Load of Post-Installed Adhesive Anchor, AIJ's JAR, Vol. 87, No. 802, pp. 1278-1287, 2023.

[4] H. Gao, A. Satoh, Behavior of Epoxy Adhesive Anchor Fixed in Large Drilled-hole Subject to Tension, Construction and Building Materials, Vol.461, pp.1-14, 2025.

[5] Y. Li, B. Winkler, A. Eckstein, Failure Analysis of Anchoring Systems in Concrete, VIII International Conference on Computational Plasticity, COMPLAS VIII, pp. 1-4, 2005.

[6] J. Barnat and M. Bajer, Analysis of Bonded Anchor in Combined Concrete-Bond Failure Mode, Recent Researches in Geography, Geology, Energy, Environment and Biomedicine, pp. 364-367, 2013.

[7] P. Upadhyaya, S. Kumar, Pull-out capacity of adhesive anchors: Analytical solution, International Journal of Adhesion & Adhesives, Vol.60, pp.54–62, 2015.

[8] D. Wang, D. Wu, C. Ouyang, S. He, X. Sun, Simulation analysis of large-diameter post-installed anchors in concrete, Construction and Building Materials, Vol.143, pp.558–565, 2017.

[9] R. A. Cook, Behavior of chemically bonded anchors, Journal of structural engineering, Vol.119, No.9, pp.2744-2762, 1993.

[10] Y. Kasa, T. Tadokoro, D. Okamoto, T. Furuya, A discussion on pullout capacity of post-installed anchor in view of load-bearing mechanisms, Proceedings of JCI, Vol.37, No.2, pp.505-510,2015.